

Infragranular Sources of Sustained Local Field Potential Responses in Macaque Primary Visual Cortex

Alexander Maier,¹ Christopher J. Aura,¹ and David A. Leopold^{1,2}

¹Unit on Cognitive Neurophysiology and Imaging, Laboratory of Neuropsychology, National Institute of Mental Health, and ²Neurophysiology Imaging Facility, National Institute of Mental Health, National Institute of Neurological Disorders and Stroke, National Eye Institute, National Institutes of Health, Department of Health and Human Services, Bethesda, Maryland 20892

A local field potential (LFP) response can be measured throughout the visual cortex in response to the abrupt appearance of a visual stimulus. Averaging LFP responses to many stimulus presentations isolates transient, phase-locked components of the response that are consistent from trial to trial. However, stimulus responses are also composed of sustained components, which differ in their phase from trial to trial and therefore must be evaluated using other methods, such as computing the power of the response of each trial before averaging. Here, we investigate the basis of phase-locked and non-phase-locked LFP responses in the primary visual cortex of the macaque monkey using a novel variant of current source density (CSD) analysis. We applied a linear array of electrode contacts spanning the thickness of the cortex to measure the LFP and compute band-limited CSD power to identify the laminar sites of persistent current exchange that may be the basis of sustained visual LFP responses. In agreement with previous studies, we found a short-latency phase-locked current sink, thought to correspond to thalamocortical input to layer 4C. In addition, we found a prominent non-phase-locked component of the CSD that persisted as long as the stimulus was physically present. The latter was relatively broadband, lasted throughout the stimulus presentation, and was centered $\sim 500 \mu\text{m}$ deeper than the initial current sink. These findings demonstrate a fundamental difference in the neural mechanisms underlying the initial and sustained processing of simple visual stimuli in the V1 microcircuit.

Introduction

A visual stimulus that appears abruptly on the retina generates a burst of synchronous activity in the primary visual cortex. This evoked onset response can be detected as an electrical potential waveform on the scalp (Berger, 1929), on the pial surface (Caton, 1875), or directly within the cortex (Adrian and Matthews, 1934), with the last measurement often termed the local field potential (LFP). Despite the potential contribution of distant neural events, some aspects of the evoked LFP responses exhibit a high degree of spatial specificity and can therefore be considered a measure of local processing (Liu and Newsome, 2006; Gieselmann and Thiele, 2008; Katzner et al., 2009). Current source density (CSD) analysis, a technique used to estimate the spatial profile of ionic flow across cellular membranes, has identified the laminar specificity of synaptic events contributing to evoked responses in the primary visual cortex. Specifically, a stimulus presentation is followed by a short-latency current sink in layer 4C that reflects the synchronized thalamocortical input into that layer, which is followed by a sequence of current sinks in the

supragranular and infragranular layers (Mitzdorf and Singer, 1979; Rappelsberger et al., 1982; Mitzdorf, 1985; Schroeder et al., 1991, 1992; Givre et al., 1994). This flow of information is consistent with the known anatomical microcircuitry of the primary visual cortex (Mitzdorf, 1985; Gilbert, 1993).

Standard CSD analysis begins with averaging the LFP waveform over a large number of stimulus presentations, based on data from multiple laminar positions collected simultaneously. Combining many presentations is important for increasing the signal-to-noise ratio of the inherently noisy CSD method. However, such trial averaging has the additional consequence of focusing analysis on time-locked (“phase-locked”) components of the stimulus response, since any response components that are not strictly locked in time to the stimulus onset will tend to cancel out. The origins and significance of phase-locked LFP responses are presently a topic of active research (Shah et al., 2004; Karmos et al., 2008) (for review, see Makeig et al., 2004). Here, we focus on the origins of the non-phase-locked component of the stimulus response, which is sometimes called the “induced” response (Tallon-Baudry and Bertrand, 1999; Lachaux et al., 2000). In contrast to the phase-locked response, which typically decays away after a few hundred milliseconds, the non-phase-locked response can persist as long as the stimulus is present. Using a novel variant of CSD analysis derived from multichannel LFP recordings in the primary visual cortex (V1) of fixating macaque monkeys, we demonstrate a sustained, non-phase-locked CSD response that lasts throughout the duration of a prolonged (1.5 s) stimulus presentation. We observed this response in a range of frequency bands, with the largest overall magnitude in the infra-

Received Oct. 26, 2009; revised Nov. 29, 2010; accepted Dec. 3, 2010.

This work was supported by the Intramural Research Programs of the National Institute of Mental Health, National Institute for Neurological Disorders and Stroke, and the National Eye Institute. We thank Katy Smith for technical assistance.

C. J. Aura's present address: Comprehensive Neuroscience Center, University of Alabama Birmingham, Birmingham, AL 35294.

Correspondence should be addressed to David A. Leopold, National Institutes of Health, Department of Health and Human Services, 49 Convent Drive, 1E21, MSC 4400, Bethesda, MD 20892. E-mail: leopoldd@mail.nih.gov.

DOI:10.1523/JNEUROSCI.5300-09.2011

Copyright © 2011 the authors 0270-6474/11/311971-10\$15.00/0

granular layers, centered $\sim 500 \mu\text{m}$ below the initial layer 4C current sink elicited by the stimulus onset. The findings suggest that V1 microcircuitry is engaged in a fundamentally different manner during the initial and sustained processing of a simple visual stimulus.

Materials and Methods

Subjects. Two healthy adult male monkeys (*Macaca mulatta*, B and E) were used in the study. All procedures followed National Institutes of Health guidelines, were approved by the Animal Care and Use Committee of the National Institute of Mental Health, and were conducted with great care for the comfort and well being of the animals.

Surgery. The monkeys were implanted with a custom-designed fiber-glass head holder under sterile surgical procedure using isoflurane anesthesia (1.5–2.0%). The head holders were affixed to the skull using transcranial ceramic screws (Thomas Recording), Copalite varnish (Cooley & Cooley) to inhibit scar tissue growth underneath the implant, and self-curing denture acrylic (Lang). In a subsequent surgery, a craniotomy was performed and covered by a custom-made plastic recording chamber implanted over V1. To target the preselected cortical region of V1 during surgery, we used the Brainsight frameless stereotaxy system (Rogue Research), guided by high-resolution (0.5 mm isotropic voxel size) anatomical magnetic resonance images acquired in a 4.7 T scanner (Bruker BioSpin). Animals received antibiotics (ketoprofen) and analgesics (buprenorphine and acetaminophen) postoperatively.

Neurophysiological recordings. Laminar LFP responses were collected during 18 recording sessions (11 of which were from monkey B). During each session, data were recorded while the animals executed a simple fixation task while a visual stimulus was presented on the screen (see below). Recordings were performed inside a radiofrequency-shielded booth. All recording sites were from dorsal V1, several millimeters posterior to the lunate sulcus, corresponding to the parafoveal region of the visual field close to the vertical meridian. Recordings were performed using a 24-contact microelectrode with an intercontact spacing of 100 μm (Neurotrack), with contact impedances varying between 0.3 and 0.5 M Ω . The multicontact electrode was manually lowered into cortex using a custom-designed microdrive. Local field potentials (defined as extracellular voltage fluctuations in the frequency range between 1 and 100 Hz) were amplified and recorded using the Plexon MAP system (Plexon). The LFP was amplified by a factor of 1000, digitized at 1 kHz for data collection and subsequently downsampled to 250 Hz after low-pass filtering with an eighth-order, bidirectional, zero-phase Chebyshev type 1 filter with a cutoff frequency of 100 Hz, and converted into microvolts as a function of time. Receptive fields were mapped based on audible multiunit responses in the beginning of the recording session using vertical and horizontal bars of variable length that could be freely moved across the presentation screen using a computer mouse.

We determined the laminar position of the multicontact electrode by computing the visually evoked potential (VEP) and CSD profiles for brief visual stimulation during a passive fixation task. During this task, the black screen went white quasiperiodically (between ~ 50 and ~ 300 times with a frequency of ~ 1 Hz, depending on the monkeys' behavior) for a period of 100 ms and returned to its black state while the monkey had to maintain fixation on the screen. Initial depth adjustments were made during each session based on the reversal of the initial VEP, which was visible on-line on a computer monitor. More precise determination of the position was then achieved off-line based on the current source density elicited by these responses, allowing for precise intersession electrode alignment (Maier et al., 2010) (see Fig. 3).

Data analysis. All neurophysiological data were processed and analyzed using custom-written Matlab code (The MathWorks). Band-limited power (BLP) of both the LFP and CSD was computed by bandpass filtering the appropriate signal using a second-order, bidirectional, zero-phase Chebyshev type 1 bandpass filter (frequency ranges indicated in the text; also see Fig. 2 for an outline of analysis steps). The band-limited signals were then full-wave rectified, providing a measure of time-varying amplitude, or signal power (more precisely, the square

root of the power), in each frequency band. BLP signals were computed on a trial-by-trial basis, and then averaged over trials.

Current source density was computed by applying a standard algorithm (according to the second spatial derivative estimate of the laminar LFP time series) along with the iCSD toolbox for Matlab (Pettersen et al., 2006). A value of 0.4 S/m was taken as a measure of cortical conductivity (Logothetis et al., 2007) to approximate current source density in units of nanoamperes per cubic millimeter. The band-limited power of the CSD (BLP_{CSD}) was computed from the CSD signal in the same way that BLP was computed from the LFP signal, involving steps of bandpass filtering, rectification, and averaging over trials (see Fig. 2B).

One difference between BLP and BLP_{CSD} signals is the sensitivity of the latter to small artifacts. Specifically, the computation of the second spatial derivative for the CSD makes it highly susceptible to small sources of noise, such as vibration and relative movement that can differentially affect the upper channels. Moreover, unlike the LFP signal, the CSD at each position is computed using adjacent LFP contacts, meaning that noise at a superficial channel can affect the CSD computation at a deeper channel. As a result, and based on artifacts observed on single trials that were most likely attributable to relative motion at and above the dura mater measured in the uppermost contacts, we took the conservative approach of excluding spatial positions $>600 \mu\text{m}$ above the zero point in layer 4 (see below) from the BLP_{CSD} analysis.

Significance of stimulus responses versus the corresponding unstimulated (fixation-only) condition was computed in the following manner using the nonparametric Wilcoxon rank sum test, although nearly identical results were obtained with paired *t* tests: The mean stimulus response of each session was computed by considering the mean signal value (BLP or BLP_{CSD}, respectively) within a time window ranging from 0.5 and 1.5 s after stimulus onset (or the respective points in time following fixation during the fixation-only control condition). For each electrode position, we then tested whether the mean stimulus responses across sessions were significantly different from the mean fixation-only responses across sessions at a level $p < 0.05$ (Bonferroni corrected for multiple comparisons). At each cortical depth, a significant difference, corresponding to a significant stimulus response, is designated by an asterisk (see Figs. 5, 7; supplemental Figs. 3, 6, available at www.jneurosci.org as supplemental material).

Visual stimulation. Visual stimuli were generated using OpenGL-based custom-written software (ESS/STIM; copyright Dr. D. Sheinberg, Brown University, Providence, RI) running on industrial PCs (Kontron) with NVIDIA Quadro FX 3000 graphics boards. Stimuli were presented on either a single 18 inch TFT monitor placed in front of the animals (NEC MultiSync LCD 1860NX with a 1024 \times 768 resolution) or two 27 inch TFT monitors (X2Gen MV2701; 1024 \times 768 resolution) with a diagonal of 32 inches (X2Gen MV2701; 1024 \times 768 resolution) mounted on opposite walls of the test box at a viewing distance of 80 cm and a custom-made mirror stereoscope mounted in front of the head-restrained animal.

Task and paradigm. In the main stimulus presentation task, the animals kept continuous gaze at a small (0.01 dva) spot at the center of the screen as a binocular, bright white luminance patch centered on the receptive field, typically having a radius of 1–2 dva (as stimulus size was adjusted to the receptive field and varied between sessions), and was presented at an eccentricity ~ 4 dva (exact location varied with electrode position). Only the initial 1.5 s of stimulus presentation are analyzed in the present study, as the later periods of the trial were used for a different study. In the fixation-only condition, the animal was required to simply maintain fixation for several seconds, without any additional stimuli present on the screen. The animals were required to fixate within a 1- to 2-dva-diameter fixation window for 6 s to receive juice reward. If a monkey broke fixation, the trial was aborted and reinitiated after a short delay of 100–800 ms. The animal's eye movements were monitored and recorded using an infrared light sensitive camera and commercially available eye tracking software (EyeLink II; SR Research). There were no specific attention requirements in this task, other than to maintain fixation on the central point.

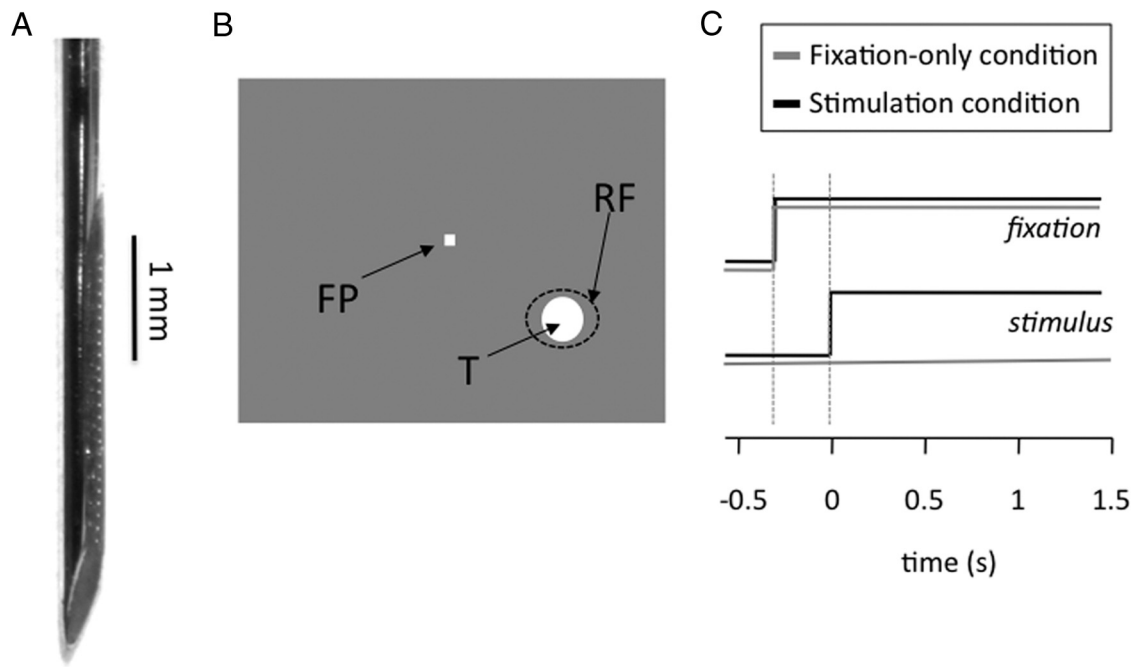


Figure 1. Recording technique and stimulus paradigm. **A**, Data were collected with a 24 channel linear recording array, with 100 μm spacing between electrode contacts. Each day, the electrode was inserted perpendicular to the cortical surface of V1 so that the lowermost contacts were in the white matter and the uppermost were superficial to the pia mater. **B**, The receptive field was mapped manually using the minimal response field technique for spiking responses. The receptive field generally resided in the lower visual field contralateral to the V1 recording chamber. The stimulus consisted of a uniformly white disk (FP, fixation spot; RF, receptive field; T, target visual stimulus). **C**, Exactly 300 ms after the monkey acquired fixation, the stimulus appeared on the monitor covering the receptive field and remained present as the monkey fixated for 1.5 s.

Results

Our main goal was to investigate the neural current sources underlying sustained stimulus responses in V1. We approached this using a novel variant of the laminar CSD technique to estimate the power of fluctuating ionic currents at different cortical depths. Each day, we inserted a multicontact linear electrode array perpendicular to the cortical surface and measured LFP responses simultaneously from 24 sites spaced at equal 100 μm intervals between the pia mater and the white matter (Fig. 1A). Once the electrode was inserted, we performed three sequential procedures. First, we manually mapped the spatial position of the receptive field using moving bars presented on the screen while listening to multiunit activity through an audio monitor (Fig. 1B,C) (see Materials and Methods). Second, we adjusted the electrode depth and collected a brief data file that was used to determine the final laminar position for intersession alignment (see below, Electrode positioning and intersession alignment). Third, we conducted the main experimental testing paradigm.

The main paradigm consisted of the presentation of a single binocular, white disk, which appeared for 1.5 s in the receptive field position of the recording site, as the monkey fixated a small point in the center of the screen (Fig. 1B,C) (see Materials and Methods). Stimulating with a binocular luminance patch minimized the contribution of site-specific selectivity for orientation and ocular dominance that characterizes the functional architecture of the primary visual cortex, allowing us to optimally average equivalent laminar response profiles measured at different tangential positions. In addition to stimulated trials, there were also unstimulated control trials, in which the fixation point remained alone at the center of the screen with no stimulus in the receptive field. In all cases, the monkeys were simply required to maintain fixation on the central point to obtain their juice reward. Throughout the data collection, the LFP was measured and recorded from each of the 24 electrode contacts.

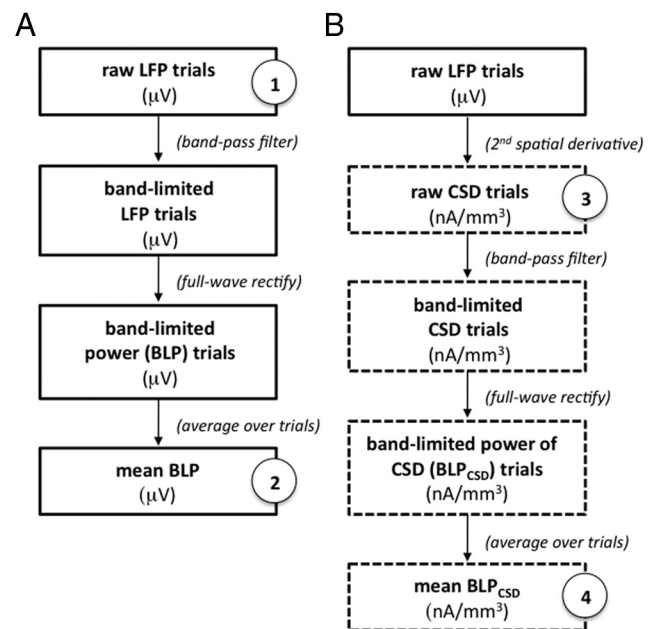


Figure 2. Framework for computing the four main signals analyzed in the present study. **A**, LFP signals. (1) Raw LFP trials, as recorded directly. (2) Mean BLP trials, after bandpass filtering and rectification of the LFP. **B**, CSD signals. (3) Raw CSD trials, derived from the LFP trials by taking the second spatial derivative. (4) BLP_{CSD} trials, after bandpass filtering and rectification of the CSD.

In analyzing the conventional (transient, phase-locked) and sustained (late, non-phase-locked) components of the stimulus responses, the LFP data were processed according to analysis pipelines shown in Figure 2 and described briefly here. (1) Phase-locked LFP. Following the conventions normally used to evaluate

visually evoked responses, the initial, phase-locked LFP was computed as the mean extracellular voltage trace averaged over many trials. This was done separately for each channel. (2) Band-limited power of the LFP (BLP). The non-phase-locked LFP response (sometimes called the induced response) was analyzed by examining the band-limited power of the signal in standard electroencephalographic frequency ranges (Leopold et al., 2003). Note that, because the early portion of the visual response constitutes a mixture of phase-locked and non-phase-locked responses, we focused our analysis on the late portion (beginning 500 ms or later) (see below), after the phase-locked response had decayed away. (3) Phase-locked CSD. The phase-locked CSD was analyzed in the conventional manner, using the mean LFP trace across trials of each channel as the input to the CSD algorithm. (4) Band-limited power of the CSD (BLP_{CSD}). The sustained, non-phase-locked CSD response was examined as a function of frequency by applying the band-limited power technique as in (2). For the BLP_{CSD} , the CSD was first computed for each trial, at which point the trials were filtered and rectified before averaging. As in (2), we focused on the late, sustained portion of the response, after the phase-locked component had decayed away.

In the following sections, we first describe the electrode alignment procedure using conventional phase-locked CSD. We then describe the laminar pattern of LFP power in different frequency bands using BLP analysis. Finally, we describe the laminar pattern of CSD power in different frequency bands using BLP_{CSD} analysis.

Electrode positioning and intersession alignment

At the beginning of each session, a conventional CSD paradigm was used to position the electrode relative to the initial visually evoked current sink. For this procedure, the stimulation paradigm consisted of the repeated presentation of a bright, white flashing screen ($40 \times 30^\circ$). Each flash lasted 100 ms and was separated by a 1 s (or more, depending on the monkey's behavior) interval while the monkey fixated the center of the monitor. At the beginning of this period, we positioned the electrode by adjusting its depth while we observed the raw on-line LFP response to each stimulus presentation. The electrode was adjusted to bring the reversal in the evoked LFP polarity (coarsely associated with layer 4) at or near the middle of the array.

After this initial adjustment, which ensured that the electrode contacts spanned the thickness of cortex and were in approximately the same position from session to session, we collected LFP for several minutes during a large number of stimulus presentations (at least 100). These trials were recorded and analyzed off-line using conventional CSD methods. The resulting spatio-temporal CSD profile, including the initial layer 4C current sink in response to the stimulus flash, served as the basis for the session-to-session alignment done before computing the intersession average. In some cases, this data collection was repeated at the end of the session to verify that the electrode was stable in its position (see examples in supplemental Fig. 9A, available at www.jneurosci.org as supplemental material). Note that there was a

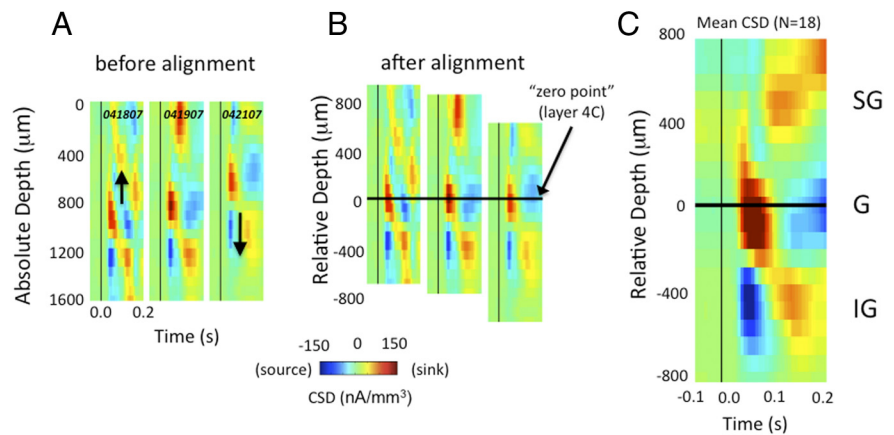


Figure 3. Aligning sessions based on a flash-evoked CSD pattern collected before the experiment. **A**, CSD computed for each session, represented on an interpolated space–time surface, with red indicating current sinks. Different sessions (consisting of recordings in different animals and cortical locations) showed initial current sinks on different electrode contacts because of the slight variability between days in manual positioning of the electrodes across the cortical thickness. **B**, Based on the CSD pattern, different sessions were shifted so that the center of the initial current sink was at the zero point, thought to correspond to layer 4C α . **C**, Mean CSD pattern after alignment (data from both monkeys, $N = 18$). SG, Supragranular; G, granular; IG, infragranular.

good correspondence of our data with other studies that have traced the initial current sink layer 4C α (Mitzdorf and Singer, 1979; Schroeder et al., 1991). Throughout the paper, we refer to this point of alignment as the “zero point” (Fig. 3).

Because the CSD method highlights second-order differences between adjacent channels (i.e., it is proportional to the second spatial derivative), it is highly susceptible to noise and artificial disturbances of the measured potential on one or more measurement points, as might accompany any instability of the electrode or the movement of the animal. We approached this issue conservatively, eliminating any sessions that (1) had significant movement artifacts or (2) did not yield a precise estimate of electrode position. Analysis was therefore restricted to 18 sessions (11 from monkey B and 7 from monkey E) in which the recordings were judged to be stable and free of artifacts. Additional details are provided in Materials and Methods.

Laminar distribution of sustained LFP responses

We first investigated the depth profile of transient and sustained LFP responses in V1 by computing BLP for several standard frequency ranges at each laminar position (Fig. 4B). As a guide to laminar positioning, Figure 4A shows the mean, phase-locked CSD response to the flashing stimulus presented during the alignment trials ($N = 18$ sessions). The initial current sink is clearly visible as a short-latency, negative deflection, which is in good agreement with previous work (Tenke et al., 1993). The red horizontal line, based on this initial sink, indicates the zero point used for intersession alignment. The panels in Figure 4B show the mean BLP response stemming from different frequency bands (columns) located at different cortical depths (rows). Specifically, the three rows correspond to the average response of three contacts in the supragranular (SG), granular (G), or infragranular (IG) laminar domains (gray lines). Responses at all individual contact positions (without averaging across laminar positions) are shown in supplemental Figure 1 (available at www.jneurosci.org as supplemental material). Within each panel, the mean and SE of the stimulated condition (colored lines) are shown along with responses during the fixation-only condition (black lines). The prominent BLP responses indicate a broadband increase in LFP power that rises quickly and persists throughout the 1.5 s of stimulus presentation. Note that the measured BLP elevation is

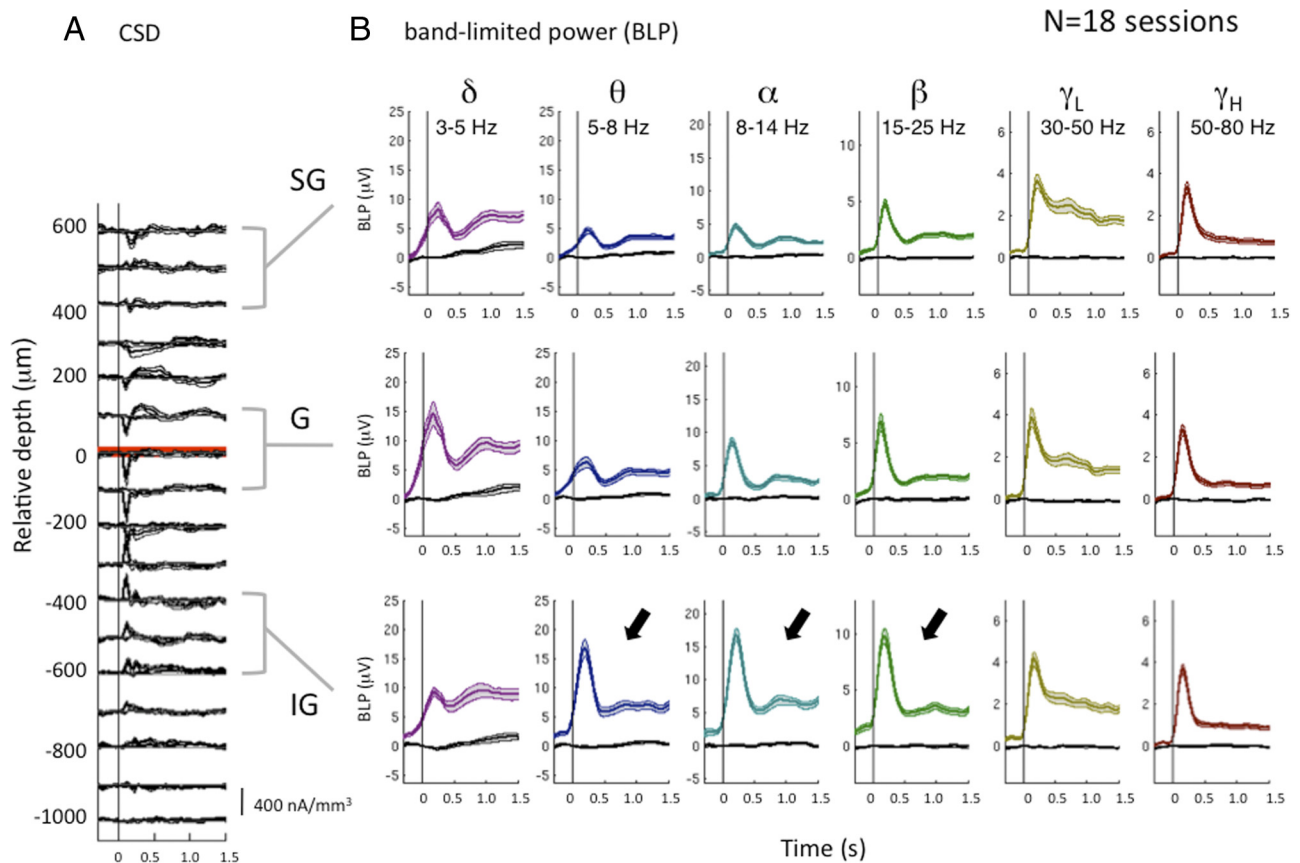


Figure 4. Laminar distribution of BLP traces relative to the stimulus-evoked CSD pattern. **A**, Mean time course of CSD deflections measured at each cortical position after the presentation of the stimulus at time $t = 0$ (gray lines, SEM; data from both monkeys, $N = 18$ sessions). **B**, Average BLP responses across three electrodes determined to be in the supragranular (SG), granular (G), and infragranular (IG) layers based on the CSD responses. Mean (\pm SEM) time courses for different frequency bands are in color, whereas the corresponding time course for unstimulated trials are in black. Frequency bands are broken down into standard electroencephalographic frequency bands. The red horizontal line corresponds to the zero point established in layer 4. Note that activity changes that precede the stimulus presentation (most pronounced for the lowest frequency ranges) are an expected artifact of the bandpass filtering process, which decreases the temporal resolution, but does not impact interpretation of the sustained response.

present in all laminar compartments. For frequencies ranging from 5 to 25 Hz, responses are stronger in the IG compartments (arrows), whereas for higher frequencies the responses are more evenly distributed across layers.

Focusing next on the magnitude of the sustained response, which is dominated by non-phase-locked components of the LFP response, we computed the mean BLP within a time window between 0.5 and 1.5 s after the stimulus onset. This was done for each of the frequency ranges and laminar positions (Fig. 5) (for the results expressed in percentage change, see also supplemental Fig. 12A, available at www.jneurosci.org as supplemental material). This analysis revealed that, for virtually all frequencies and laminar positions, there was a significant elevation in LFP power in the stimulated condition compared with the unstimulated control condition (Wilcoxon's rank sum test, $p < 0.05$) (see Materials and Methods). The equivalent prestimulation versus poststimulation comparison is shown in supplemental Figure 2 (available at www.jneurosci.org as supplemental material). The result was similar in the first versus second half of the sustained period (supplemental Figs. 3, 10, available at www.jneurosci.org as supplemental material). Note that even the deepest contacts, which, based on their distance from the initial sink, were likely located in the white matter, showed robust sustained BLP responses. These responses in the white matter highlight the nonlocal nature of LFP that follows from passive volume conduction.

Note that, in our analysis, the units of the BLP in Figures 4 and 5 are the same as those of the evoked response (microvolts). This is because we elected to rectify the signal using the absolute value (rather than the square) of the frequency-specific response of each trial. This measure of LFP magnitude is thus proportional to the square root of the LFP power. Expressing the band-limited LFP magnitude in this way provides a convenient and intuitive way to estimate the relative contribution of phase-locked and non-phase-locked LFP contribution to the response, as well as to other events and rhythms present in the raw LFP trace.

Laminar distribution of sustained CSD responses

In an effort to gain insight into the types and laminar position of synaptic processes underlying the sustained LFP responses described in the previous section, we next sought to determine the laminar distribution of current sinks and sources, not only after the initial presentation of a stimulus but also throughout its prolonged presentation. As explained in the Introduction, conventional CSD analysis is applied to average evoked responses, and thereby discards non-phase-locked components of the stimulus response. To capture non-phase-locked components that dominate the sustained response, we therefore applied the BLP approach described in the previous section to the CSD itself (Fig. 2B). Briefly, each trial was filtered into multiple frequency bands, the CSD profile was computed for each of these bands, and the resulting band-limited CSD signal was then rectified by taking

N=18 sessions

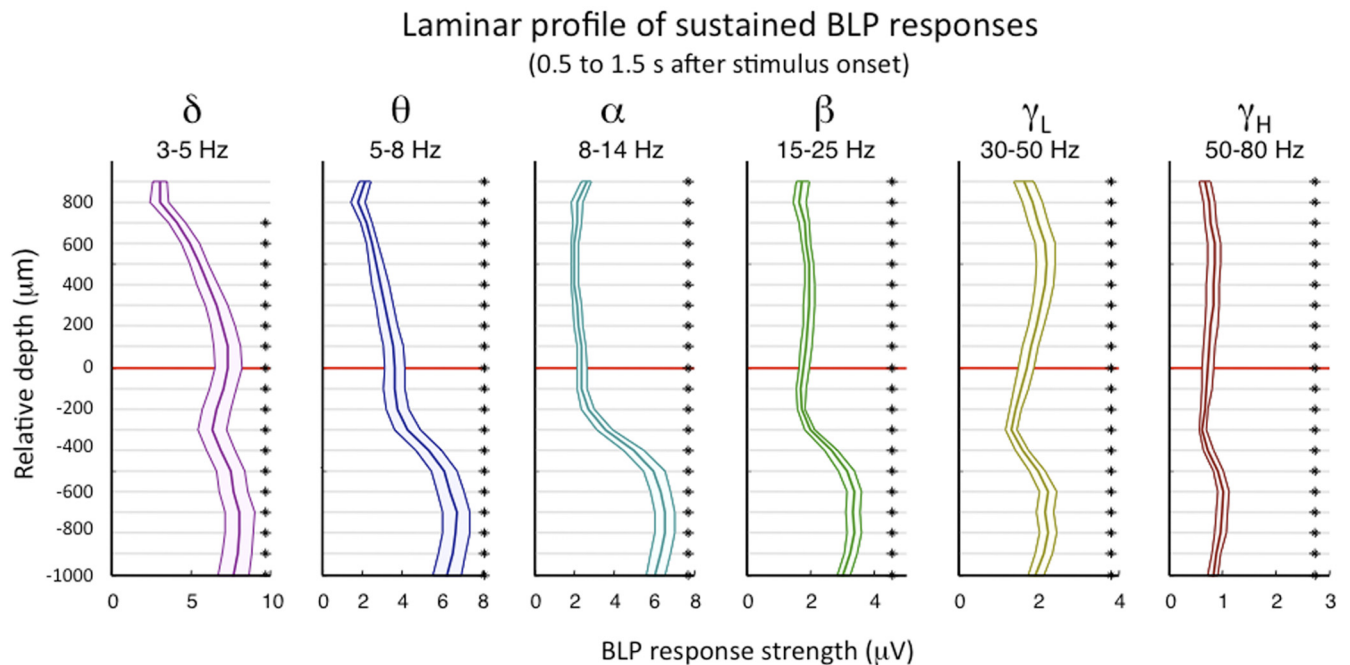


Figure 5. Laminar distribution of mean sustained BLP responses. Data were taken after the evoked, phase-locked voltage deflection had diminished (0.5–1.5 s) and therefore represent the late non-stimulus-locked component of the response. The asterisks indicate significant increases in BLP at each frequency and cortical depth (Wilcoxon's rank sum test, $p < 0.05$ after Bonferroni's correction). Note that each position showed significant increases for each frequency range, indicating a widespread, sustained increase in broadband LFP power.

the absolute value. Computing the average of each frequency range over multiple trials resulted in a family of band-limited power signals derived from the CSD (BLP_{CSD}). It is important to point out that, by rectifying the CSD signal, the polarity information inherent in the CSD (i.e., sink vs sources) is lost. This is a drawback that, among other things, leads to the combination of active sinks and adjacent passive sources, leading to a somewhat lower spatial resolution of source/sink modulation than achieved with conventional CSD analysis. Yet in our framework the downsides of this loss of spatial precision are outweighed by the merits of observing currents contributing to the non-phase-locked response components that make up the sustained response.

The BLP_{CSD} traces resulting from this analysis are shown in Figure 6, for stimulated (color) versus unstimulated (black) trials (for all channels individually, see supplemental Fig. 4, available at www.jneurosci.org as supplemental material). The SG, G, and IG zones correspond to the same electrode contact positions depicted in Figure 4. In contrast to the BLP responses shown in Figure 4B and supplemental Figure 1 (available at www.jneurosci.org as supplemental material), significant BLP_{CSD} responses were restricted in their laminar positions, with the most prominent sustained modulation in the lower granular and infragranular layers and virtually no response at more superficial positions (see supplemental Figs. 4, 10, available at www.jneurosci.org as supplemental material). Note that, because channels $>600 \mu\text{m}$ above zero were excluded from our analysis (see Materials and Methods), we were not able to measure BLP_{CSD} in the topmost superficial layers. As in the case with the BLP signal described above, we next focused on the sustained response, computing the difference between stimulated and unstimulated conditions in a window ranging from 0.5 to 1.5 s after stimulus onset. Figure 7 shows the mean sustained BLP_{CSD} response difference between stimulated and unstimulated trials (for prestimulus vs post-

stimulus comparison, see supplemental Fig. 5, available at www.jneurosci.org as supplemental material; for the results expressed in percentage change, see supplemental Fig. 12B, available at www.jneurosci.org as supplemental material). The most obvious feature is a concentration of sustained activity centered $\sim 500 \mu\text{m}$ below the zero point thought to be located in layer 4C. As with the BLP above, separately analyzing the first and second halves of the sustained time window produced similar results (supplemental Fig. 6, available at www.jneurosci.org as supplemental material). The strongest BLP_{CSD} elevation was in the delta, theta, and alpha frequency ranges, for which several deep granular and infragranular positions showed significant responses ($p < 0.05$, corrected). Some sustained modulation in the gamma range was present in the granular zone, although this modulation was also most prominent below the zero point (see supplemental Figs. 4, 12B, available at www.jneurosci.org as supplemental material). Importantly, in all but the lowest frequency range, the BLP_{CSD} response fell to zero in the upper layers, standing in sharp contrast to the BLP traces. Finally, consistent with the near absence of synaptic events in the white matter, the sustained modulation of the BLP_{CSD} fell to near zero at sites $>700 \mu\text{m}$ below the zero point.

Discussion

This study sheds new light on the generation of sustained responses in LFP power in the primary visual cortex during the prolonged presentation of visual stimuli. In computing the band-limited power of the CSD, we were able to identify an elevation of current sources and sinks within the infragranular layers. These currents may underlie the sustained elevation in non-phase-locked LFP power measured in all layers, and even in the white matter, during the presentation of a stimulus.

Although the BLP_{CSD} measure is novel in many respects, it does share some similarity to previous approaches. For example,

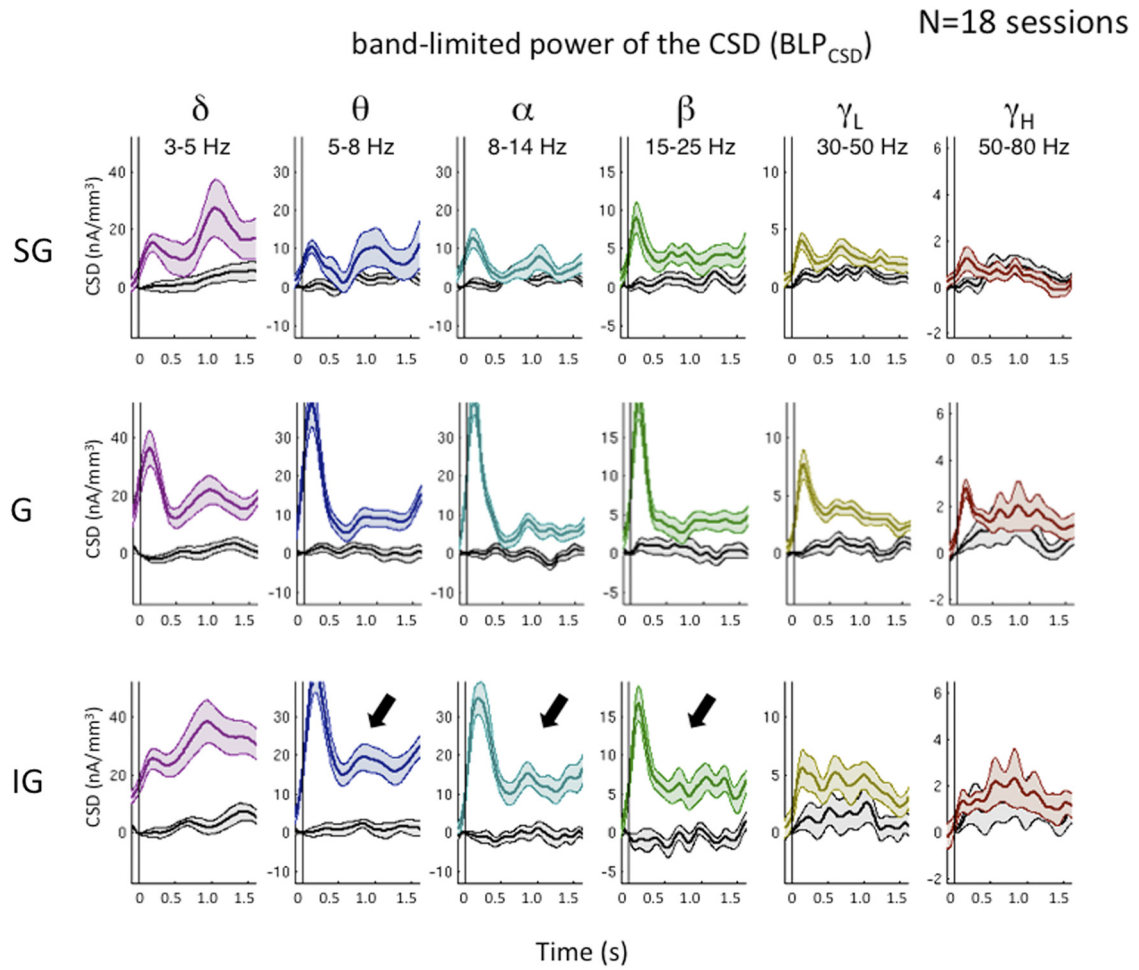


Figure 6. Laminar distribution of BLP_{CSD} traces. Mean (\pm SEM) time courses for different frequency bands are in color, whereas the corresponding time course for unstimulated trials are in black. Note the sustained responses in the lower layers for frequencies <25 Hz (arrows). Other conventions are the same as in Figure 4.

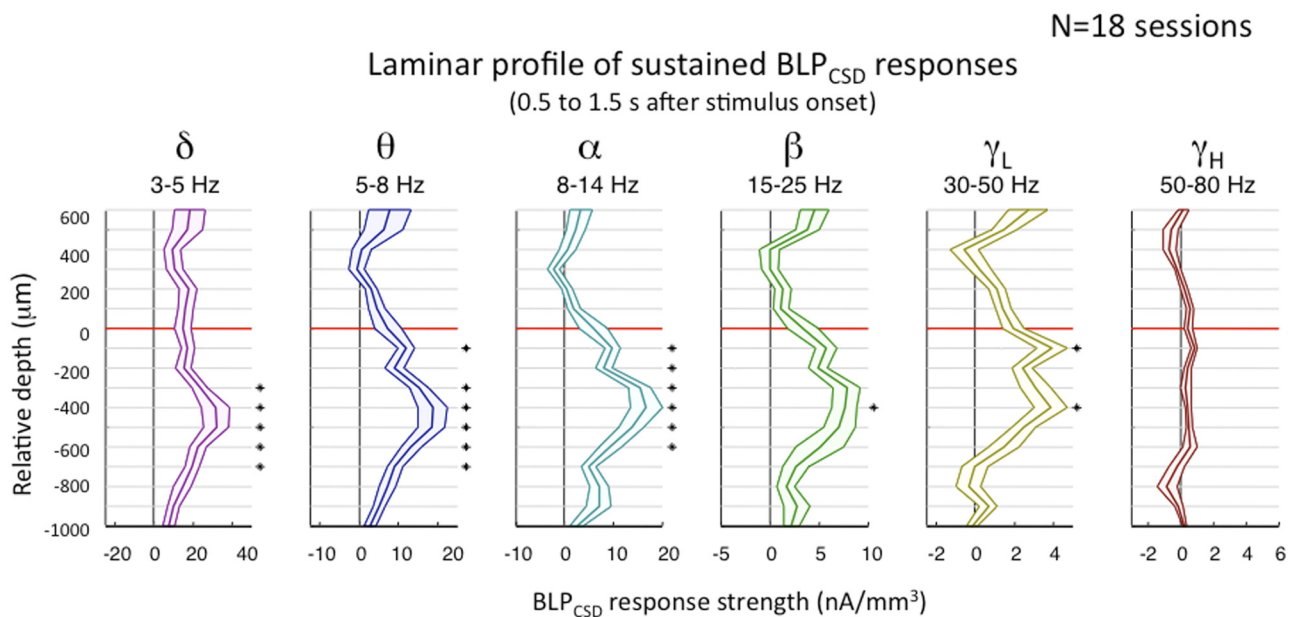


Figure 7. Laminar distribution of mean sustained BLP_{CSD} responses. Conventions are as in Figure 5. Note that, in contrast to Figure 5, only a subset of laminar positions display significant modulation of sustained activity during stimulus presentation, with most modulating sites in the infragranular layers.

the AVREC (average rectified current flow waveform) measure used previously (Mehta et al., 2000) also involves the rectification of current sinks and sources after the CSD computation. The BLP_{CSD} method is also related to the computation of instantaneous amplitude using the Hilbert transform, which has previously been used to characterize the CSD power for eye movement-related responses on a single-trial basis, in different laminar compartments (Rajkai et al., 2008). Like each of these other approaches, the BLP_{CSD} method allows for the evaluation of non-phase-locked components of a stimulus response, while at the same time providing good temporal resolution and reasonable laminar resolution. Another recent approach circumvents the alignment to the repeated presentation of stimuli by instead aligning to detected cycles of the spontaneous alpha rhythm (Bollimunta et al., 2008) or slow waves (Csercsa et al., 2010), which has the advantage of preserving the polarity of current sources and sinks, and thus maintaining high laminar resolution.

A vital aspect of the present study was the development of a paradigm to combine data from different recording sessions. Using conventional CSD analysis to identify the initial current sink in layer 4C evoked by a flashing stimulus, and then shifting the session average of each day based on the position of the electrode contacts relative to that sink, proved to be a straightforward and reliable method. This alignment enabled the precise registration and averaging across multiple recording sessions (Maier et al., 2010). Computing the inter-session average helped us to deal with the low sensitivity associated with the inherently noisy CSD signal.

Granular and infragranular origins of LFP responses

In agreement with much previous work using CSD analysis, we found that the onset of a simple visual stimulus leads to an abrupt and transient current sink. This pattern of responses has been directly linked to the underlying anatomy of primary visual cortex, and is known to reflect the retinogeniculate input to layer 4C (Mitzdorf and Singer, 1979). Our computation of BLP_{CSD} responses from the same electrode positions in the same sessions suggests that a very different mechanism underlies the sustained, non-phase-locked (induced) response. Specifically, we found that the peak BLP_{CSD} was centered $\sim 500 \mu\text{m}$ deeper than the main layer 4C current sink, in what appeared to be layer 5 (Fig. 8). If we assume that the BLP_{CSD} measure reflects some aspects of local synaptic activity, it is interesting to consider what types of synaptic connections might be involved. Based on the basic projection patterns of V1 neurons, there are at least three categories of synaptic input that might contribute as follows: (1) direct afferents from LGN relay neurons carrying information from the retina; (2) input from outside of V1, such as extrastriate visual cortex or the pulvinar, which may one way or another serve to support the V1 stimulus representation; and (3) intrinsic processing within the V1 microcircuit. We will discuss these possibilities in this order.

From a theoretical point of view, it seems inevitable that direct afferents from the LGN to V1 make some contribution to the sustained LFP response, be it direct or indirect. The type of stimulus we used is known to elicit sustained firing of neurons in the parvocellular (P) layers of the LGN (Schiller and Malpeli, 1978). P neurons project primarily to layer $4C\beta$, which in our study appeared to exhibit significant sustained BLP_{CSD} changes for several frequency ranges. Other P neurons terminate in layer 6, which also showed significant responses. Nonetheless, it seems unlikely that the LGN afferents alone are primarily responsible for the sustained currents we observed. For one, the highest

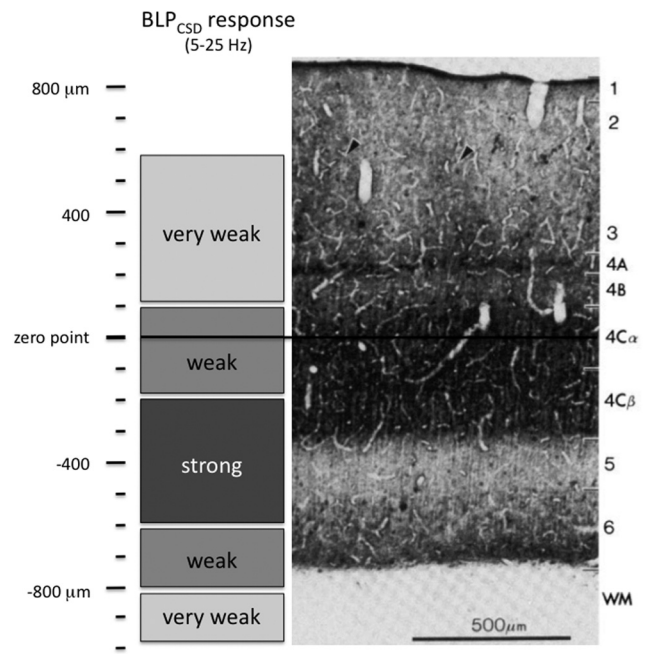


Figure 8. Summary diagram of the main finding. The most pronounced, sustained BLP_{CSD} modulation was located in the infragranular cortical layers, 300–600 μm below the zero point in layer 4, and thought to correspond to layer 5. Flanking regions in layers 4 and 6 also showed some modulation, with little or none in the supragranular layers. Histological reference slide was adapted from the study by Blasdel and Lund (1983).

BLP_{CSD} magnitude was almost certainly below layer $4C\beta$, probably in layer 5. This is difficult to reconcile with direct LGN inputs, since layer 5 is one of only two V1 layers that does not receive any LGN afferents, with the other being layer 4B (Lund, 1988; Callaway, 1998).

The second possibility is that the observed infragranular responses arise from other cortical or thalamic structures. This prospect is so general that it is impossible to rule out completely. However, as with the first possibility, the observed laminar pattern of BLP_{CSD} modulation does not seem to fit with this scenario. Although the extrastriate cortex does project some terminals into the infragranular layers, including layer 5 (Rockland and Virga, 1989) and layer 6 (Felleman and Van, 1991; Angelucci and Bullier, 2003), the majority of descending afferents from the cortex terminate in the upper layers of V1. Likewise, the main pulvinar input to V1 is to the upper layers, and particularly to layer 1 (Ogren and Hendrickson, 1977). It bears repeating that at this point we cannot rule out the presence of such currents in the upper supragranular layers, since we were only able to compute the mean BLP_{CSD} for positions up to 600 μm above the zero point.

Finally, we must consider the contribution of intrinsic cortical connections. It is known that the majority of synapses in a cortical column arise from intrinsic projections, rather than from the thalamus or distant cortical areas (Douglas et al., 1989; Douglas and Martin, 2007). Even in layer $4C\beta$ of macaque V1, $<10\%$ of the synapses originate from LGN afferents (Peters et al., 1994). The majority of the other synapses within a cortical column arise from intrinsic, local projections. The fact that CSD reliably registers a localized current sink after the abrupt onset of a stimulus indicates that even the minority of synapses that arise from the LGN, when strictly time-locked to an external event, can produce a sizable current. Nonetheless, it may be that, under other conditions, such as during the sustained period after the dissipation of

the phase-locked response, the intrinsic corticocortical currents predominate. It is possible that such currents involve a different set of laminar connections and are particularly important for the maintenance of an enduring stimulus. Previous anatomical, physiological, and theoretical work has pointed to recurrent excitation as an important feature of the cortical microcircuit (Douglas et al., 1995). Such recurrent excitation might be promoted by the continued presentation of a stimulus, but is unlikely to bear a strict temporal relationship to its onset. It is intriguing to speculate that such intrinsic excitation, say between layers 2/3 and 5 (Gilbert and Wiesel, 1983; Callaway, 1998, 2004; Douglas and Martin, 2004), driven by the prolonged presentation of a stimulus, might be responsible for the non-phase-locked responses we found in the infragranular layers.

Measuring alternating cortical currents

What neural processes underlie the observed BLP_{CSD} responses? The most direct interpretation is that the elevation of the BLP_{CSD} in response to the presentation of a stimulus represents an increase in the overall magnitude of bidirectional current exchange between the intracellular and extracellular compartments. The BLP_{CSD} method is essentially a convergence of the BLP and CSD methods, deriving the advantages (and disadvantages) of each. It is important to emphasize that the BLP_{CSD} measures alternation of current, rather than the magnitude of direct current. In that sense, it is similar to other measures of LFP power, such as the computation of its band-limited power. To our knowledge, no previous cortical LFP or scalp EEG study has examined the current source basis of sustained stimulus responses. Whether the estimation of fluctuating local currents is a valuable tool remains to be determined. If it can provide an estimation of “synaptic power” that is traceable to either information processing or energetics within the cortical column, this measure could be important for understanding the enigmatic relationship between LFP measurements and hemodynamic responses, which is presently the subject of intense investigation (Logothetis, 2002, 2008; Viswanathan and Freeman, 2007; Maier et al., 2008; Sirotin and Das, 2009).

Finally, a few additional caveats need to be mentioned regarding this method. First, like all CSD methods, this approach employs a number of assumptions, such as isotropic current in the tangential direction, and uniform conductivity, neither of which is strictly accurate for the cerebral cortex. Second, even if the electrodes are properly shifted relative to the initial current sink, averaging over days may not make sense for some questions, since the electrode penetrations may be different in their positions relative to the cortical functional architecture. In V1, different tangential positions correspond most obviously to shifts in ocular dominance and orientation selectivity. To minimize inter-session variability, we therefore selected stimuli that were likely to elicit responses approximately equally as a function of cortical position (i.e., binocular luminance patches). Whether the laminar profile of BLP_{CSD} responses depends on the specific stimulus used is a matter for future investigation. Given these caveats, it was reassuring that the session mean of the evoked CSD response was highly consistent between electrode penetrations and animals and closely resembled that which has been previously reported in the literature. It was also important to observe that the BLP_{CSD} responses, in contrast to the BLP responses, were absent in the white matter, reflecting the fact that, although there may be fluctuating voltages measured in this tissue, these voltage fluctuations do not reflect local current exchange.

References

- Adrian ED, Matthews BH (1934) The interpretation of potential waves in the cortex. *J Physiol* 81:440–471.
- Angelucci A, Bullier J (2003) Reaching beyond the classical receptive field of V1 neurons: horizontal or feedback axons? *J Physiol Paris* 97:141–154.
- Berger H (1929) Über das elektroencephalogramm des menschen. *Arch Psychiatr Nervenkr* 87:527.
- Blasdel GG, Lund JS (1983) Termination of afferent axons in macaque striate cortex. *J Neurosci* 3:1389–1413.
- Bollimunta A, Chen Y, Schroeder CE, Ding M (2008) Neuronal mechanisms of cortical alpha oscillations in awake-behaving macaques. *J Neurosci* 28:9976–9988.
- Callaway EM (1998) Local circuits in primary visual cortex of the macaque monkey. *Annu Rev Neurosci* 21:47–74.
- Callaway EM (2004) Feedforward, feedback and inhibitory connections in primate visual cortex. *Neural Netw* 17:625–632.
- Caton R (1875) Electrical currents of the brain. *J Nerv Ment Dis* 2:610.
- Csercsa R, Dombóvári B, Fabó D, Wittner L, Eross L, Entz L, Sólyom A, Rásonyi G, Szucs A, Kelemen A, Jakus R, Juhos V, Grand L, Magony A, Halász P, Freund TF, Maglóczy Z, Cash SS, Papp L, Karmos G, et al. (2010) Laminar analysis of slow wave activity in humans. *Brain* 133:2814–2829.
- Douglas RJ, Martin KA (2004) Neuronal circuits of the neocortex. *Annu Rev Neurosci* 27:419–451.
- Douglas RJ, Martin KA (2007) Recurrent neuronal circuits in the neocortex. *Curr Biol* 17:R496–R500.
- Douglas RJ, Martin KA, Witteridge D (1989) A canonical microcircuit for neocortex. *Neural Comput* 1:480–488.
- Douglas RJ, Koch C, Mahowald M, Martin KA, Suarez HH (1995) Recurrent excitation in neocortical circuits. *Science* 269:981–985.
- Felleman DJ, Van Essen DC (1991) Distributed hierarchical processing in the primate cerebral cortex. *Cereb Cortex* 1:1–47.
- Gieselmann MA, Thiele A (2008) Comparison of spatial integration and surround suppression characteristics in spiking activity and the local field potential in macaque V1. *Eur J Neurosci* 28:447–459.
- Gilbert CD (1993) Circuitry, architecture, and functional dynamics of visual cortex. *Cereb Cortex* 3:373–386.
- Gilbert CD, Wiesel TN (1983) Functional organization of the visual cortex. *Prog Brain Res* 58:209–218.
- Givre SJ, Schroeder CE, Arezzo JC (1994) Contribution of extrastriate area V4 to the surface-recorded flash VEP in the awake macaque. *Vision Res* 34:415–428.
- Lakatos P, Karmos G, Mehta AD, Ulbert I, Schroeder CE (2008) Entrainment of neuronal oscillations as a mechanism of attentional selection. *Science* 320:110–113.
- Katzner S, Nauhaus I, Benucci A, Bonin V, Ringach DL, Carandini M (2009) Local origin of field potentials in visual cortex. *Neuron* 61:35–41.
- Lachaux JP, Rodriguez E, Martinerie J, Adam C, Hasboun D, Varela FJ (2000) A quantitative study of gamma-band activity in human intracranial recordings triggered by visual stimuli. *Eur J Neurosci* 12:2608–2622.
- Leopold DA, Murayama Y, Logothetis NK (2003) Very slow activity fluctuations in monkey visual cortex: implications for functional brain imaging. *Cereb Cortex* 13:422–433.
- Liu J, Newsome WT (2006) Local field potential in cortical area MT: stimulus tuning and behavioral correlations. *J Neurosci* 26:7779–7790.
- Logothetis NK (2002) The neural basis of the blood-oxygen-level-dependent functional magnetic resonance imaging signal. *Philos Trans R Soc Lond B Biol Sci* 357:1003–1037.
- Logothetis NK (2008) What we can do and what we cannot do with fMRI. *Nature* 453:869–878.
- Logothetis NK, Kayser C, Oeltermann A (2007) In vivo measurement of cortical impedance spectrum in monkeys: implications for signal propagation. *Neuron* 55:809–823.
- Lund JS (1988) Anatomical organization of macaque monkey striate visual cortex. *Annu Rev Neurosci* 11:253–288.
- Maier A, Wilke M, Aura C, Zhu C, Ye FQ, Leopold DA (2008) Divergence of fMRI and neural signals in V1 during perceptual suppression in the awake monkey. *Nat Neurosci* 11:1193–1200.
- Maier A, Adams GK, Aura C, Leopold DA (2010) Distinct superficial and deep laminar domains of activity in the visual cortex during rest and stimulation. *Front Syst Neurosci* 4:1–11.

- Makeig S, Debener S, Onton J, Delorme A (2004) Mining event-related brain dynamics. *Trends Cogn Sci* 8:204–210.
- Mehta AD, Ulbert I, Schroeder CE (2000) Intermodal selective attention in monkeys. II: Physiological mechanisms of modulation. *Cereb Cortex* 10:359–370.
- Mitzdorf U (1985) Current source-density method and application in cat cerebral cortex: investigation of evoked potentials and EEG phenomena. *Physiol Rev* 65:37–100.
- Mitzdorf U, Singer W (1979) Excitatory synaptic ensemble properties in the visual cortex of the macaque monkey: a current source density analysis of electrically evoked potentials. *J Comp Neurol* 187:71–83.
- Ogren MP, Hendrickson AE (1977) The distribution of pulvina terminals in visual areas 17 and 18 of the monkey. *Brain Res* 137:343–350.
- Peters A, Payne BR, Budd J (1994) A numerical analysis of the geniculocortical input to striate cortex in the monkey. *Cereb Cortex* 4:215–229.
- Pettersen KH, Devor A, Ulbert I, Dale AM, Einevoll GT (2006) Current-source density estimation based on inversion of electrostatic forward solution: effects of finite extent of neuronal activity and conductivity discontinuities. *J Neurosci Methods* 154:116–133.
- Rajkai C, Lakatos P, Chen CM, Pincze Z, Karmos G, Schroeder CE (2008) Transient cortical excitation at the onset of visual fixation. *Cereb Cortex* 18:200–209.
- Rappelsberger P, Pockberger H, Petsche H (1982) The contribution of the cortical layers to the generation of the EEG: field potential and current source density analyses in the rabbit's visual cortex. *Electroencephalogr Clin Neurophysiol* 53:254–269.
- Rockland KS, Virga A (1989) Terminal arbors of individual “feedback” axons projecting from area V2 to V1 in the macaque monkey: a study using immunohistochemistry of anterogradely transported *Phaseolus vulgaris*-leucoagglutinin. *J Comp Neurol* 285:54–72.
- Schiller PH, Malpel JG (1978) Functional specificity of lateral geniculate nucleus laminae of the rhesus monkey. *J Neurophysiol* 41:788–797.
- Schroeder CE, Tenke CE, Givre SJ, Arezzo JC, Vaughan HG Jr (1991) Striate cortical contribution to the surface-recorded pattern-reversal VEP in the alert monkey. *Vision Res* 31:1143–1157.
- Schroeder CE, Tenke CE, Givre SJ (1992) Subcortical contributions to the surface-recorded flash-VEP in the awake macaque. *Electroencephalogr Clin Neurophysiol* 84:219–231.
- Shah AS, Bressler SL, Knuth KH, Ding M, Mehta AD, Ulbert I, Schroeder CE (2004) Neural dynamics and the fundamental mechanisms of event-related brain potentials. *Cereb Cortex* 14:476–483.
- Sirotin YB, Das A (2009) Anticipatory haemodynamic signals in sensory cortex not predicted by local neuronal activity. *Nature* 457:475–479.
- Tallon-Baudry C, Bertrand O (1999) Oscillatory gamma activity in humans and its role in object representation. *Trends Cogn Sci* 3:151–162.
- Tenke CE, Schroeder CE, Arezzo JC, Vaughan HG Jr (1993) Interpretation of high-resolution current source density profiles: a simulation of sub-laminar contributions to the visual evoked potential. *Exp Brain Res* 94:183–192.
- Viswanathan A, Freeman RD (2007) Neurometabolic coupling in cerebral cortex reflects synaptic more than spiking activity. *Nat Neurosci* 10:1308–1312.